THE JOURNAL OF PHYSICAL CHEMISTRY C
A JOURNAL OF THE AMERICAN CHEMICAL SOCIETY

pubs.acs.org/JPCC

Article

Revisiting Ammonia Oxidation Reaction on Polycrystalline Pt: A Rotating Ring Disk Electrode-Based Investigation

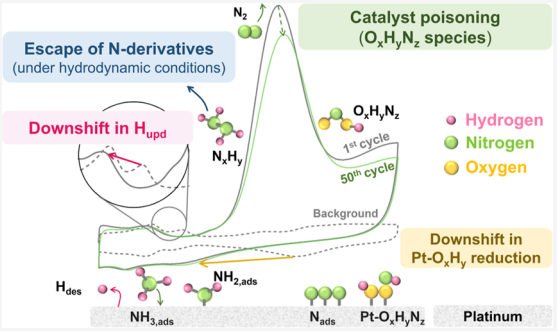
Amruta Iyer, Sagar Chauhan, Bradley P. Ladewig, and Manoj Neergat*

Cite This: https://doi.org/10.1021/acs.jpcc.6c04500

Read Online

ACCESS | Metrics & More | Article Recommendations | Supporting Information

ABSTRACT: Ammonia oxidation reaction (AOR) is investigated on polycrystalline Pt-disk and Pt-black catalysts in 0.1 M KOH in a rotating ring-disk electrode (RRDE) configuration in the potential range of 0.05−1.10 V (vs reversible hydrogen electrode, RHE). The effects of electrode porosity, ammonia concentration, convective mass transport, and the upper and lower potential limits of the voltammograms on AOR are investigated. The RRDE voltammograms in both NH_3-free and NH_3-containing supporting electrolytes, and chronoamperograms (CAs) with intermittent rotation at regular intervals, are recorded to understand the AOR mechanism and poisoning by the intermediates. A downshift of ∼60−70 mV (at ∼50 μA cm^{-2}) in the onset potential of AOR is accompanied by a distinct downshift (∼130 mV) in the H adsorption/desorption peaks of the Pt {100} sites on increasing the NH_3 concentration from 1.0 mM to 1.0 M. The results indicate that certain characteristic features observed in CA and RRDE voltammograms have contributions from the unintentional dissolved oxygen content in the bulk electrolyte.



1. INTRODUCTION

Electrochemical oxidation of ammonia has various applications in energy-conversion devices, such as NH_3-based electrolyzers (for green hydrogen production), fuel cells, sensors, and in wastewater remediation processes.[1−6] Although the ammonia oxidation reaction (AOR) has a thermodynamically appealing potential of ∼0.06 V, it is kinetically sluggish, thereby impeding the device performance. Consequently, electrocatalytic studies on the AOR are crucial to improve the fundamental and mechanistic understanding of the process.

The two widely deliberated pathways for AOR (Gerischer-Maurer (G-M) and Oswin-Salomon (O−S) mechanisms) differ on one key account. The G-M mechanism considers N_{ads} as a surface poison that inhibits AOR, whereas[7] the O−S mechanism hypothesizes N_{ads} to be the key precursor for N_2 evolution.[7,8] More importantly, according to the G-M mechanism, AOR proceeds through the dimerization of the dehydrogenated NH_3 molecules to form N_xH_y intermediates. While density functional theory (DFT)-based computational methods and differential electrochemical mass spectrometry (DEMS)-based experimental studies reported in the literature advocate the prevalence of the G-M mechanism on several transition metal-based catalysts, recent studies suggest subtle deviations.[9−12] These include decoupled proton−electron transfer steps and active involvement of NO species as AOR intermediates rather than their conventional classification as an unwanted byproduct.[13,14]

AOR has mostly been investigated on Pt-based catalysts (primarily due to its adherence to the Sabatier's principle) with a noteworthy focus on monocrystalline Pt.[9,13,15−18] Among the various Pt facets, Pt (100) has been widely examined for AOR due to its ability to stabilize intermediate species.[13,16,19,20] On the contrary, theoretical and in situ spectroscopic studies indicate the low activity of Pt (111) and (110) facets toward AOR. This is perhaps due to either the feeble adsorption of NH or firm binding of N species, resulting in surface poisoning.[15,16] Likewise, the lack of adherence to the Sabatier's principle causes most metals to fall on either extreme of the volcano plot and results in their inability to effectively oxidize NH_3.[10] However, in the alloy form, such elements are reported to catalyze AOR effectively.[21] For instance, the onset of AOR depicts a negative shift of ∼100 mV on $Pt_{1-x}Ir_x$ and $Pt_{1-x}Ru_x$ alloys as compared to pure Pt.[22] Due to the limited availability and associated expense of Pt catalysts, the focus of research has also shifted toward nonprecious metal-based catalysts for AOR. While Ru-, Fe-, and Cu-based homogeneous catalysts show promising activity in aqueous and non-aqueous media, they are largely challenged by concomitant side reactions, catalyst precipitation, and recycling affecting their large-scale implementation.[23−26] Among heterogeneous catalysts, Ni has shown

Received: July 7, 2026
Revised: September 25, 2026
Accepted: October 5, 2026

ACS Publications © XXXX American Chemical Society

Downloaded from pubs.acs.org/jpccck/article-pdf/doi/10.1021/acs.jpcc.6c04500/68939061/acs.jpcc.6c04500.pdf by HIGHER COLLEGES OF TECHNOLOGY, Bradley Ladewig on 03 November 2026

some activity, yet it suffers from sluggish AOR kinetics, catalyst poisoning, and competing side reactions.[27−29]

The sheer number of possible reaction intermediates and their consequent pathways make the mechanistic and kinetic understanding of AOR on Pt highly complex. Thus, contrasting observations reported in the literature regarding the mass transport dependence of AOR; while some publications have reported an increase in the AOR peak current with rotation, experiments conducted at higher concentrations of NH_3 feature a fall in the anodic peak current with convection.[4,20,30] Both these observations are loosely tied to the AOR mechanism; however, a detailed investigation of their occurrence and underlying mechanism has not yet been reported. Further, the addition of NH_3 in the bulk electrolyte significantly alters the characteristic features of polycrystalline Pt, including (but not limited to) a downshift in the H_{UPD} region and oxide reduction, which remain largely underexplored. Some studies in the literature attribute a certain peak that occurs before AOR to the desorption of H and the adsorption of NH_3.[13,14] However, such reports contest the observed downshift in the H_{UPD} region and require further verification. Further, the occurrence of concomitant side reactions in the same potential window as that of AOR has often been disregarded, leading to the misinterpretation of the recorded electrochemical data. Therefore, fundamental challenges and disagreements regarding AOR persist despite significant advancements, necessitating a revisit of the AOR on Pt to better understand its kinetics and mechanism.

Therefore, AOR on polycrystalline Pt electrodes is investigated using a rotating ring disk electrode (RRDE) assembly. The dependence of AOR on NH_3 concentration, extrinsic mass transport, dissolved oxygen content and upper- and lower-potential limits of the voltammograms was investigated using cyclic voltammetric techniques. Chronoamperograms (CAs) with intermittent rotation were recorded to understand the effect and extent of poisoning by intermediate species. The trend in the ring current (i_R) in NH_3-free and NH_3-containing supporting electrolytes was also analyzed.

2. EXPERIMENTAL SECTION

2.1. Materials

Platinum black (Pt-black, HiSPEC 1000, Johnson Matthey) was purchased from Alfa Aesar. Ammonium hydroxide (NH_4OH, 28−30%), sulfuric acid (H_2SO_4, 98 wt %), potassium hydroxide (KOH, ≥85%), and 2-propanol ($(CH_3)_2CHOH$, ≥99.5%) were purchased from Merck. Nafion (5 wt % in a mixture of lower aliphatic alcohols and water) was purchased from Sigma-Aldrich. All the materials were used as is without further purification. High-purity argon (Ar) and oxygen (O_2) were obtained from Med Gas N Equipment, India. Deionized (DI) water (18.2 MΩ cm) from Direct-Q 3 water purification system (Merck Millipore) was used for all the experiments.

2.2. Electrode Preparation

A Pt-black coated glassy carbon disk (GCD) and Pt-disk were used as working electrodes in the RRDE configuration. Both assemblies were purchased from Pine Research Instrumentation with a disk area of 0.196 cm^2 and a platinum ring area of 0.110 cm^2. The GCD and Pt-disk were mirror polished with 0.05 μm alumina suspension (Buehler) and then sonicated for 5 min in DI water and dried in air at room temperature before use. To prepare the Pt-black electrode, 5 mg of Pt-black catalyst was added to a solution containing 5 mL of DI, 10 mL of isopropyl alcohol (IPA), and 10 μL of Nafion. The solution was then ultrasonicated for 30 min to obtain the catalyst ink (0.33 mg mL^{-1}).[31] Subsequently, 30 μL of the ultrasonically dispersed catalyst suspension was pipetted onto the clean GCD substrate, yielding a catalyst loading of 51 $\mu g\ cm^{-2}$.

2.3. Electrochemical Characterization

All electrochemical measurements were performed in a standard electrochemical cell in a RRDE configuration. Double junction Hg/Hg_2SO_4 (saturated K_2SO_4) and single junction Hg/HgO (saturated KOH) were used as reference electrodes in acidic and alkaline media, respectively. Nevertheless, all potentials in this study are reported against the reversible hydrogen electrode (RHE). A graphite rod in a glass tube with a sintered glass frit bottom (to prevent cross-contamination of the working electrode by the products generated at the surface) filled with the supporting electrolyte of the same concentration (to maintain conductivity) was used as the counter electrode.

Cyclic voltammograms (CVs) were recorded using a Wave Driver 200 bipotentiostat and rotator (Pine Research Instrumentation). Prior to subjecting the working electrode to an alkaline environment, it was activated by cycling in an Ar-saturated 0.5 M H_2SO_4 electrolyte at a scan rate of 50 mV s^{-1} in the potential range of 0.05 to 1.15 V until reproducible voltammograms were obtained (Figure S1a). Subsequently, the working electrode was conditioned in 0.1 M KOH in the potential range of 0.05 to 1.1 V until reproducible CVs were obtained (Figure S1b). Prior to the chronoamperometric measurements on the disk and ring, the disk was held at 0.45 V in Ar-purged 0.1 M KOH to electrochemically reduce the unintentionally dissolved O_2 content in the bulk electrolyte to water. A detailed explanation about the necessity of such a protocol is discussed in the manuscript in Section 3.6. AOR voltammograms were then recorded in Ar-saturated 0.1 M KOH electrolyte (with various concentrations of NH_3) at a scan rate of 20 mV s^{-1} in the above-mentioned potential range. The detailed procedure of preparing the ammoniacal solution is mentioned in the Supporting Information (S2). The ring electrode was held in the double layer region (0.45 V vs RHE in NH_3-free solutions and 0.35 V vs RHE in 1 M NH_3 containing solutions), where the oxidation or reduction of N-based derivatives could occur without interference from background AOR currents. The ring-disk voltammograms were recorded at various rotation rates (0.0, 400.0, 900.0, 1600.0, and 2400.0 rpm), and the details are explicitly mentioned wherever required. CAs were recorded to test the effect of rotation by holding the electrode at 0.65 V (all other details are mentioned wherever necessary). The ring-disk electrode was periodically cleaned after each experiment by cycling it in 0.5 M H_2SO_4 to remove the adsorbed OH^-, NH_3, and N-based adsorbates. Fresh ammonia solution was prepared ahead of each experiment due to its tendency to vaporise when exposed to air over a long period of time.[13]

3. RESULTS AND DISCUSSION

3.1. Effect of Electrode Porosity and NH_3 Concentration on AOR

To study the influence of NH_3 concentration on AOR, CVs were recorded on both Pt-disk and Pt-black in a range of NH_3 concentrations. Mathematically, the relationship between the current density and the bulk concentration of redox-active species is described by eq 1.[32]

$$j_{AOR} = nFkC^*_{NH_3} \quad (1)$$

Here, j_{AOR} is the AOR current density, n the number of electrons involved in the half-reaction, F the Faraday's constant, k the rate constant, and $C^*_{NH_3}$ is the bulk concentration of NH_3.

It is inferred from the equation that an increase in $C^*_{NH_3}$ should loosely translate to a rise in the anodic peak current. Consequently, Figure 1 depicts an increase in the AOR peak current density (j^{peak}_{AOR}) with an increase in $C^*_{NH_3}$ (in accordance

Downloaded from pubs.acs.org/jpccck/article-pdf/doi/10.1021/acs.jpcc.6c04500/6893906l/acs.jpcc.6c04500.pdf by HIGHER COLLEGES OF TECHNOLOGY, Bradley Ladewig on 03 November 2026

https://doi.org/10.1021/acs.jpcc.6c04500
J. Phys. Chem. C XXXX, XXX, XXX−XXX

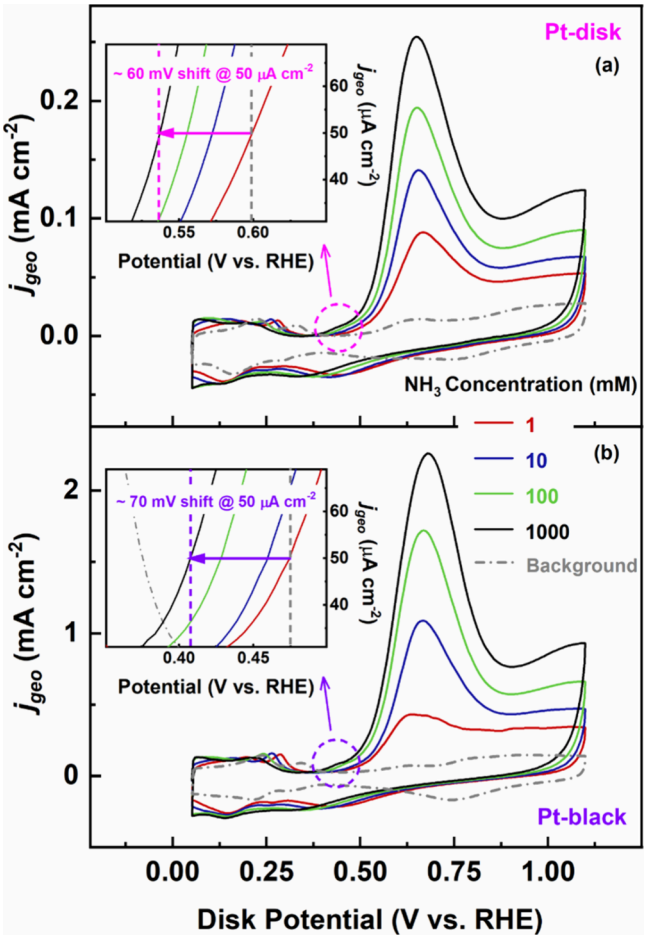


Figure 1. CVs of AOR on (a) Pt-disk and (b) Pt-black coated GCD electrode (0.196 cm^2) in argon-saturated 0.1 M KOH with various concentrations of NH_3 at a scan rate of 20 mV s^{-1}. The insets in (a) and (b) show the shift in the potential at a fixed current density of ~50 μA cm^{-2} with increasing NH_3 concentration on Pt-disk and Pt-black, respectively.

with the data reported in the literature) on both Pt-disk and Pt-black.[3,4] Notably, the increment in the j_{AOR}^{peak} with concentration follows a gradient pattern, being more prominent at low concentrations of NH_3 and diminishing further (as better visualized in Figure S3). This can be attributed to the saturation of active sites with adsorbates on increasing in the concentration of NH_3. Consequently, the current begins to saturate at ~1.0 M NH_3 as maximum coverage of active sites is achieved.

Interestingly, a shift of ~60 mV on Pt-disk and ~70 mV on Pt-black is observed at 10 μA cm^{-2} as the NH_3 concentration changes from 1.0 mM to 1.0M. This agrees with the distinct negative shift in the onset of AOR reported by Koper et al. on Pt {111}.[15] This shift in the onset is attributed to the strong adsorption and higher coverage of NH_3 on Pt.

To investigate the effect of electrode porosity, AOR was recorded on polycrystalline Pt-disk and Pt-black (Figure 1a,b). The surface roughness for both electrodes was quantified by eq 2.

$$\text{roughness} = \frac{A_{ECSA}}{A_{Geometric}} \quad (2)$$

Here, A_{ECSA} stands for the electrochemical active surface area (ECSA), which was calculated by integrating the H_{UPD} currents for both Pt-black and Pt-disk (Figure S4).[33] $A_{Geometric}$ corresponds to the apparent area of the disk electrode (0.196 cm^2).

The measured roughness factor for Pt-black is ~10 times the roughness factor obtained for Pt-disk. Consequently, the current densities for Pt-black are substantially higher than those for non-porous polycrystalline Pt. Accordingly, all further experiments were performed using 1.0 M NH_3 on the Pt-black catalyst.

3.2. Effect of Extrinsic Mass Transport on AOR

To investigate the effect of the convective mass transport on the j_{AOR}^{peak}, CVs were recorded at two different concentrations on the Pt-black catalyst (Figure 2). At 1 mM NH_3 concentration,

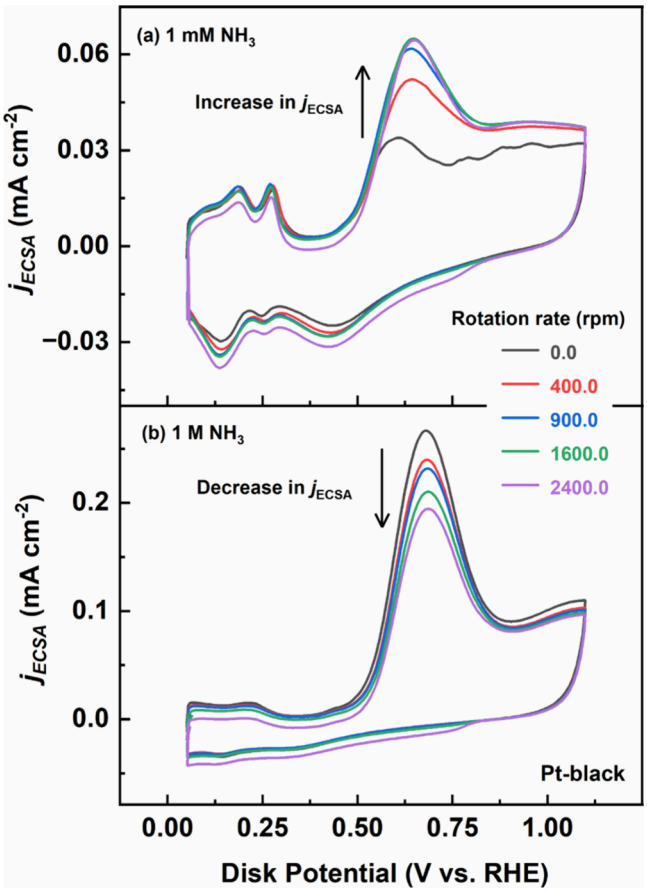


Figure 2. AOR voltammograms on Pt-black in (a) 1.0 mM and (b) 1.0 mM NH_3 in Ar-saturated 0.1 M KOH at a scan rate of 20 mV s^{-1} at various rotation rates.

j_{AOR}^{peak} increases with the rotation rate (ω) until saturation in the peak current is attained (Figure 2a). However, a contrary trend is observed at 1000 mM NH_3; j_{AOR}^{peak} decreases with increase in ω (Figure 2b).

Both these observations were independently reported in the literature; however, the origin of the conflicting trends remains unresolved.[20,30] The general notion about the reasons for the decrease in the j_{AOR}^{peak} with ω includes catalyst poisoning and escape of surface intermediates.[30,34] Since the obtained results (both from the literature and this study) were a consequence of different experimental conditions, and particularly, disparate concentrations of NH_3, it is apparent that the dependence of

https://doi.org/10.1021/acs.jpcc.6c04500
J. Phys. Chem. C XXXX, XXX, XXX−XXX

Downloaded from pubs.acs.org/jpcccck/article-pdf/doi/10.1021/acs.jpcc.6c04500/6893906l/acs.jpcc.6c04500.pdf by HIGHER COLLEGES OF TECHNOLOGY, Bradley Ladewig on 03 November 2026

j_{AOR}^{peak} on ω is a strong function of the available NH_3 concentration in the bulk electrolyte, among other factors as discussed below.

A review of the literature and results from this study collectively suggest that dependence of j_{AOR}^{peak} on ω at different concentrations of NH_3 may stem from the interplay among four factors: convective mass transport, strong adsorption of certain species on the active sites, escape of weakly bound adsorbates from the disk electrode and occurrence of concomitant side reactions.

First, the general effect of convective mass transport on peak current densities is well-established. As the ω increases, the influx of the NH_3 species to the disk electrode becomes increasingly facile resulting in a positive contribution to the i_{AOR}^{peak} (i_{ω}^{+}).

Second, several computational and spectroscopic studies indicate the amplified formation of N_{ads} at higher potentials on Pt (>0.6 V).[10,12,13] These surface nitrides (Pt−N) have an adsorption energy of approximately −394 kJ mol^{-1} on Pt, leading to their irreversible adsorption on Pt due to their stable nature.[12] Further, over-oxidation of NH_3 in aqueous electrolytes can generate $O_xH_yN_z$ species that strongly bind to the catalyst (discussed in detail in the following sections). The formation and adsorption of both N_{ads} and $O_xH_yN_z$ species collectively contribute to catalyst poisoning as is evident from the decrease in the j_{AOR}^{peak} with cycling (Figure S5). Thus, some active sites become unavailable to catalyze AOR (contributing to i_{ads}^{-}), thereby resulting in a net decrease in the disk current.

Third, most experimental studies in the literature agree with the G-M mechanism that proposes N-based derivatives.[9,11,13,15] These intermediates, if bulky in nature, may get displaced from the disk electrode under rotation, leading to a loss of active species from the catalyst surface (contributing to i_{escape}^{-}) and thus a lesser reaction current.

Fourth, along with the desired reactions, certain unwanted side reactions that occur in the same potential window can negatively impact the disk current. Oftentimes, mere purging of the bulk electrolyte with Ar does not suffice, as it still leads to an inevitable presence of dissolved oxygen in the electrolyte. As a result, the contribution of the oxygen reduction reaction (ORR) to the measured currents (as the potential window for ORR overlaps with that of AOR) cannot be neglected. The extent of O_2 dissolution and its influence on the experimental results become apparent in the NH_3-free supporting electrolyte and in the measured ring current (i_{ring}), as discussed later in the manuscript.

Thus, the net current can be described by eq 3.

$$i_{AOR}^{peak} = i_{\omega}^{+} + i_{ads}^{-} + i_{escape}^{-} + i_{ORR}^{-} \quad (3)$$

Here, i_{AOR}^{peak} is the net current on the disk, i_{ω}^{+} corresponds to a positive contribution to the disk current due to an increase in rotation rate, i_{ads}^{-} and i_{escape}^{-} represent the current contributions due to strong adsorption of certain chemical species and detachment of weakly bound intermediates, respectively, and i_{ORR}^{-} corresponds to the contribution to the current due to the ORR that occurs simultaneously with AOR within the experimental potential range. The superscripts indicate whether the contribution has a positive (+) or negative (−) influence on the net current.

It is important to note that eq 3 includes contributions from various factors that are not mutually additive or necessarily independent of each other. For instance, an increase in ω can contribute to a simultaneous increase in the NH_3 and O_2 flux, and therefore, a rise in both AOR and ORR currents. Thus, eq 3 is largely phenomenological that solely identifies the numerous contributions to the peak current and is not quantitative in nature.

On the disk, however, AOR currents (at 1000 mM NH_3) are much more dominant in the experimental potential range, and hence the ORR contributions can be treated as trivial. Thus, the net oxidation current is collectively determined by i_{ω}^{+}, i_{ads}^{-}, and i_{escape}^{-} contributions.

Based on the observations in Figure 2a, it is hypothesized that at low concentrations of NH_3, there is a surplus availability of free Pt sites to catalyze AOR and i_{ads}^{-} is negligible. Thus, the current contribution by i_{ω}^{+} far exceeds that of i_{ads}^{-}, and i_{escape}^{-}, leading to a net increase in the current.

At 1000 mM NH_3 concentration, the surface coverage of Pt active sites by NH_3 molecules approaches saturation (as can be visualized from the saturating peak current densities at higher NH_3 concentrations in Figure S6c). The oxidation of these molecules naturally leads to a higher fractional coverage by AOR intermediates on the catalyst sites. Additionally, a higher fraction of intermediates form as a consequence of increased reactant supply to the disk electrode due to an increase in the rotation rate. While some species (such as N_{ads} and $O_xH_yN_z$) bind too strongly to the catalyst surface (contributing to i_{ads}^{-}), others coalesce to form bulkier species and eventually detach, (i_{escape}^{-}). Thus, under the conditions of saturation of active sites by NH_3 species, i_{ads}^{-} and i_{escape}^{-} factors become significant in influencing the net current.

The influence of rotation rate on i_{AOR}^{peak} was recorded for NH_3 concentrations ranging from 0.5 mM to 1.0 M (Figure S6). In the low concentration regime (0.5 mM to 2.0 mM) the j_{AOR}^{peak} increased with ω while at high bulk concentrations (greater than 30.0 mM) a consistent decrease was observed. In the intermediate concentration range of 2.0 mM to 30.0 mM, no monotonic trend was observed. The behavior of the j_{AOR}^{peak} with ω was due to the interplay of various factors i_{ω}^{+}, i_{ads}^{-}, and i_{escape}^{-} as discussed above.

3.3. Downshift in H_{UPD} Region in the Presence of NH_3

Figure 3 presents the effect of NH_3 concentration on the hydrogen underpotential deposition (H_{UPD}) region of Pt-black (dashed gray line). The redox peaks A_1/C_1 (~0.27 V) and A_2/C_2 (~0.35 V) correspond to the hydrogen adsorption/desorption ($H_{ads/des}$) on {110} and {100} step sites of Pt, respectively.[35,36] A distinct negative shift of ~55 mV in the peak potentials of A_2 is observed as 1 mM NH_3 is introduced to the supporting electrolyte (Figure 3a). Further, the shift and distortion in the H_{UPD} peaks are found to be a strong function of the NH_3 concentration (Figure 3b−d).

The addition of NH_3 to the supporting electrolyte renders a significant downshift in the potential of the hydrogen desorption peaks, and the extent of the downshift of peak A_1 is summarized in Table 1. At a concentration of 1000 mM NH_3, peak A_2 (corresponding to Pt{100} and {111} step sites) downshifts substantially to the position of A_1 (corresponding to Pt{110} sites), whereas the latter becomes obscure in the experimental potential window.

The consistent downshift of the $H_{ads/des}$ peaks observed with an increase in the NH_3 concentration suggests the competing effect of NH_3 adsorption in the H_{UPD} region. While this observation is reported in the literature, the accompanying suppression and distortion of the $H_{ads/des}$ peaks are not well

Downloaded from pubs.acs.org/jpcccck/article-pdf/doi/10.1021/acs.jpcc.6c04500/68939061/acs.jpcc.6c04500.pdf by HIGHER COLLEGES OF TECHNOLOGY, Bradley Ladewig on 03 November 2026

https://doi.org/10.1021/acs.jpcc.6c04500
J. Phys. Chem. C XXXX, XXX, XXX−XXX

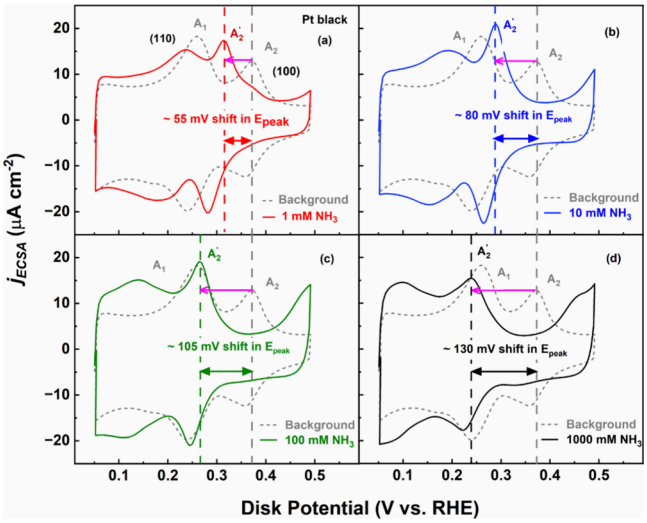


Figure 3. H_{UPD} region of Pt-black in the NH_3-free (gray dashed lines) and NH_3-containing supporting electrolytes ((a) 1.0 mM, (b) 10.0 mM, (c) 100.0 mM, and (d) 1000.0 mM NH_3) in the potential range of 0.05 to 0.5 V at a scan rate of 20 mV s^{-1}.

Table 1. Downshift in the Peak Potentials of H Desorption on Pt{100} Sites with Increase in NH_3 Concentration

NH_3 concentration (mM)	$E_{peak,A1}$ (V vs RHE)	$\Delta E_{peak,A1}$ (mV)
0 (background)	0.369	
1	0.314	55
10	0.289	80
100	0.264	105
1000	0.239	130

addressed.[12,37,38] Since the adsorption of NH_3 on Pt occurs by virtue of its lone pair of electrons, no electrochemical electron transfer step takes place. Thus, while a suppression of the $H_{ads/des}$ currents is expected, a shift in the potentials is not explained. An analogous effect is reported in the presence of benzene on Pt.[39]

In electrolytic solutions containing high concentrations of NH_3 (1000 mM), $H_{ads/des}$ occur at potentials as low as ~0.23 V (as is evident from Figure 3). In comparison, some literature reports suggest that H desorption followed by NH_3 adsorption can occur at potentials as high as ~0.45 V.[13,14] The inferences from Figure 3 suggest that this feature at 0.45 V does not originate from H_{des}. A detailed description of this feature is presented in the subsequent sections.

3.4. Downshift in Oxide Region in the Presence of NH_3

With an increase in the NH_3 concentration, an enhancement in the charge of the oxide region in the form of a broad capacitive feature is observed (shaded region in Figure 4). Since this feature is a function of NH_3 concentration and occurs exclusively in the presence of NH_3, it is attributed to the strong adsorption of N-based derivatives of the form $O_xH_yN_z$.

In the backward scan, the standard reductive feature of Pt−O_xH_y is downshifted by ~420 mV in the presence of NH_3 (inset of Figure 4). The reductive feature at ~0.4 V is subtle and broad. The downshift and suppressed currents indicate that the adsorbed species in the oxide region are not purely Pt−O_xH_y, but rather N-based derivatives ($O_xH_yN_z$).

DEMS studies reported in the literature suggest a likely formation of N-based oxygenated species at higher potentials

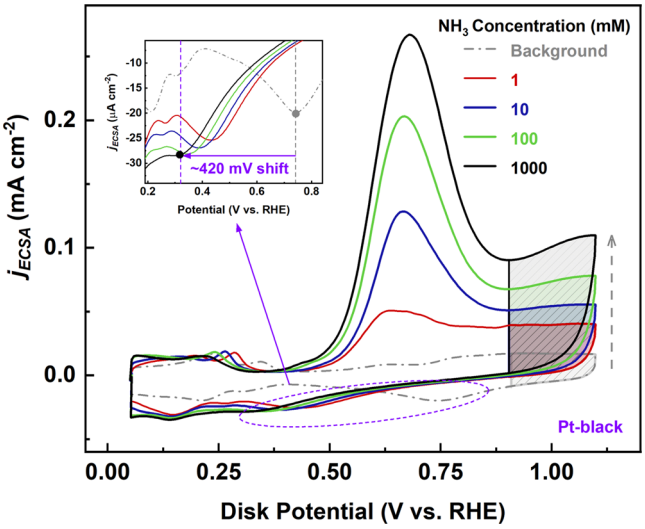


Figure 4. Cyclic voltammograms of AOR on Pt in Ar-saturated 0.1 M KOH solution containing different concentrations of NH_3. The shaded profile depicts the enhancing current in the oxide region, and the inset corresponds to the shift in the oxide reduction peak with increasing concentration of ammonia.

(>0.6 V_{RHE}) due to the overlap of Pt−O_xH_y formation and AOR.[40,41] Therefore, there is a strong likelihood that the feature in the reverse scan (in the potential range of 0.3 to 0.6 V) corresponds to the reduction of adsorbates of the form $O_xH_yN_z$.

To understand the occurrence of the reductive and oxidative features, voltammograms with varying upper- and lower-potential limits were recorded, and the results are presented in the following section.

3.5. Influence of Varying Upper and Lower Potential Limits on AOR Features

The CVs of AOR on Pt-black with different upper potential limits in 1000 mM NH_3-containing supporting electrolyte are shown in Figure 5a. As the scan progresses to various upper potential limits, the reductive features (in the reverse scan) begin to appear, corresponding to specific oxidative processes (in the forward scan) occurring within that potential range. The electrode was cycled in 0.5 M H_2SO_4 after the upper potential limit experiments to measure the change in the ECSA. The ECSA of the electrodes recovered to near baseline values after cycling in acid (Figure S7). Table 2 summarizes a brief description of the oxidative and reductive features, and their corresponding potentials.

Although a significant AOR current is recorded with both 0.65 and 0.9 V as the upper potential limits, peak C_4 (at ~0.35 V) becomes noticeable only when the latter potential is reached. The formation of Pt oxides (Pt−O_xH_y) occurs at potentials >0.75 V, and the characteristic oxide reduction peak occurs in the range of 0.45 to 1.1 V (Figure S1b). However, in the presence of NH_3, a significant downshift of the oxide reduction feature is observed and is attributed to the reduction of adsorbates of the form $O_xH_yN_z$ (discussed previously).

When the scan is reversed at 1.1 V, a further downshift in the H adsorption peak is observed as C_2^* takes shape, and C_2 disappears.

A significant shift in the A_1/C_1 and A_2/C_2 redox peaks (corresponding to$H_{ads/des}$ on Pt {110} and {111}/{100} sites, respectively) is observed with the addition of NH_3 (detailed

Downloaded from pubs.acs.org/jpccck/article-pdf/doi/10.1021/acs.jpcc.6c04500/6893906l/acs.jpcc.6c04500.pdf by HIGHER COLLEGES OF TECHNOLOGY, Bradley Ladewig on 03 November 2026

https://doi.org/10.1021/acs.jpcc.6c04500
J. Phys. Chem. C XXXX, XXX, XXX−XXX

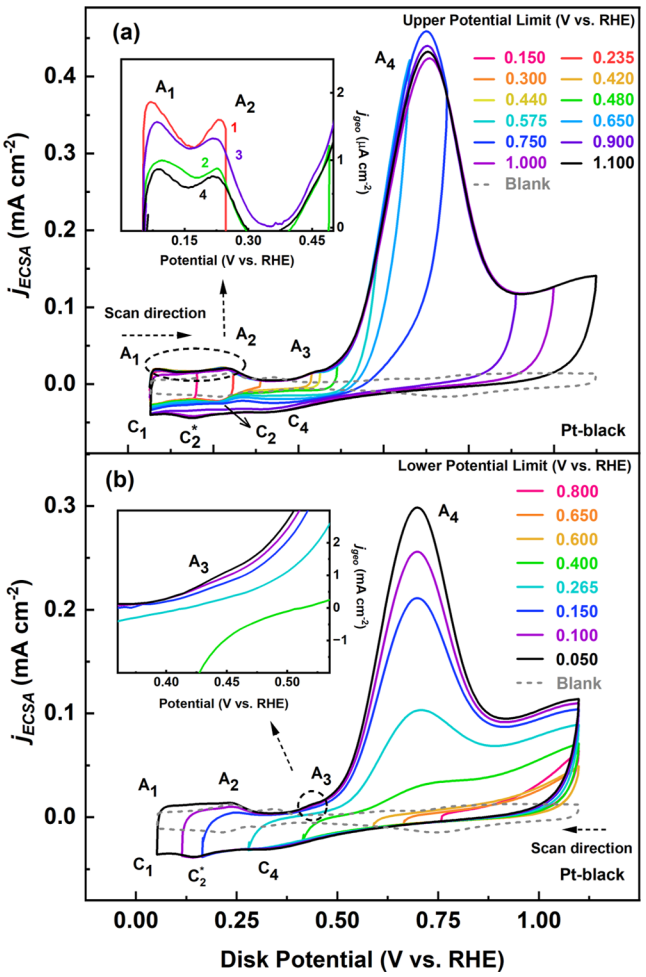


Figure 5. Voltammograms of AOR (1000 mM NH_3) on Pt-black with different (a) upper- and (b) lower-potential limits in Ar-saturated 1000 mM NH_3 in 0.1 M KOH at a scan rate of 20 mV s^{-1} under static electrode conditions. The inset of (a) depicts the change in the H_{UPD} region with selected upper potential limits, and that in (b) depicts the subtle oxidative feature A_3.

discussion presented in the previous section Figure 3). A notable change in the H desorption peak current densities (A_1 and A_2) is observed in the inset of Figure 5a as the upper potential limit is varied (summarized in Table 3). Up to the upper potential limit of 0.480 V_{RHE}, NH_3 preferentially adsorbs onto the Pt sites, thereby inhibiting $H_{ads/des}$, leading to a decrease in the hydrogen desorption current densities. However, as the upper potentials are increased, the adsorbed NH_3 intermediates get further oxidized (in the forward scan). In the reverse scan, the adsorbed intermediates and products are reduced (C_4). This leads to the recovery of the surface sites and thus a rise in the current densities. However, further increase in the potential limits leads to the coverage of the Pt surface by oxygenated species, thereby causing a decrease in the ECSA.

The ammonia oxidation peak current (A_4) in the forward scan, centered at ~0.7 V_{RHE}, rises steadily as the potential in the reverse scan is extended to lower limits (Figure 5b). The combined formation of stable Pt−$O_xH_yN_z$ (at potential >0.7 V) and OH^- adsorption (at potential >0.65 V), together, prevents the adsorption of NH_3 and its oxidation in the potential window of 0.6 to 1.1 V.[42,43] As a result, the A_4 feature is indiscernible in this range (0.6 to 1.1 V) and it becomes evident when the lower potential limit in the reverse scan crosses down to 0.4 V. This also suggests the presence of a preceding step at lower potentials that is crucial for the oxidation of NH_3. With the lowering of the reversal potential, two additional small oxidative peaks become apparent at 0.45 V (A_3) and ~0.25 V (A_2) (Figure 5b inset). Here, A_2 is the previously discussed hydrogen desorption peak (Figure 3). Although a barely noticeable feature of A_3 has been previously reported, it was crudely linked to hydrogen desorption and subsequent ammonia adsorption but lacks clarity on the underlying process.

It is evident from Figure 3 that there is a notable downshift (~130 mV) in the H_{UPD} region in the presence of 1.0 M NH_3 indicating that feature A_3 does not correspond to H desorption, unlike that reported in the literature.[13,14] The other alternative processes such as the adsorption of OH^- and K^+ ions (contributed by the electrolyte) are negligible in the measured potential range and only become significant at potentials greater than 0.55−0.6 V.[43−45] This coupled with the absence of A_3 from the voltammograms recorded in NH_3 free electrolyte collectively suggest that the feature A_3 is unlikely to have contributions from the adsorption of OH^- or K^+ ions or both. Moreover, A_4 does not occur until the lower potential limit touches ~0.4 V, indicating that A_3 is a critical step preceding to A_4. Thus, based on this analysis and considering all plausible outcomes, it can be concluded that A_3 corresponds to an electron-transfer process that becomes active in the presence of NH_3, and is crucial for AOR to occur. Hence, it is highly likely that A_3 corresponds to the dehydrogenation of NH_3.

$$NH_{3,ads} + (3 - x)OH^- \rightarrow NH_{x,ads} + (3 - x)H_2O + (3 - x)e^- \quad (4)$$

Further lowering of the initial potential leads to a consistent increase in the AOR peak current (A_4), which perhaps is a consequence of NH_3 adsorption in the H_{UPD} region, providing more time for the dehydrogenation step (eq 4). As the potentials are further lowered, NH_3 replaces the adsorbed H

Table 2. Redox Features of AOR on Pt-Black in 1.0 M NH_3 Containing 0.1 M KOH Electrolyte and Their Corresponding Potentials from This Study

redox feature	feature description	potential (V vs RHE)
A_1/C_1	H and NH_3 desorption/adsorption on {110} sites	~0.05
A_2/C_2	H and NH_3 desorption/adsorption on {100} and {111} sites	~0.25
A_3	Dehydrogenation of NH_3 (first electron transfer step), $NH_3 \rightarrow NH_2 + H^+ + e^-$	~0.45
A_4	Further oxidation of NH_3 and its intermediates	~0.7
C_4	Reduction of $O_xH_yN_z$ or N_xH_y species	~0.35
C_2^*	Modified C_2	~0.15

https://doi.org/10.1021/acs.jpcc.6c04500
J. Phys. Chem. C XXXX, XXX, XXX−XXX

Downloaded from pubs.acs.org/jpcccck/article-pdf/doi/10.1021/acs.jpcc.6c04500/6893906l/acs.jpcc.6c04500.pdf by HIGHER COLLEGES OF TECHNOLOGY, Bradley Ladewig on 03 November 2026

Table 3. H Desorption Peak Currents (A_1 and A_2) with Varying Upper-Potential Limits

label	conditions	upper limit (V vs RHE)	$j_{peak,\ A1}$ (μA cm^{-2})	$j_{peak,\ A2}$ (μA cm^{-2})
1	Initial voltammogram	~0.235	1.85	1.60
2	Before AOR	~0.480	1.00	0.90
3	After AOR	~0.9	1.55	1.30
4	After Pt−$O_xH_yN_z$ formation	~1.1	0.90	0.75

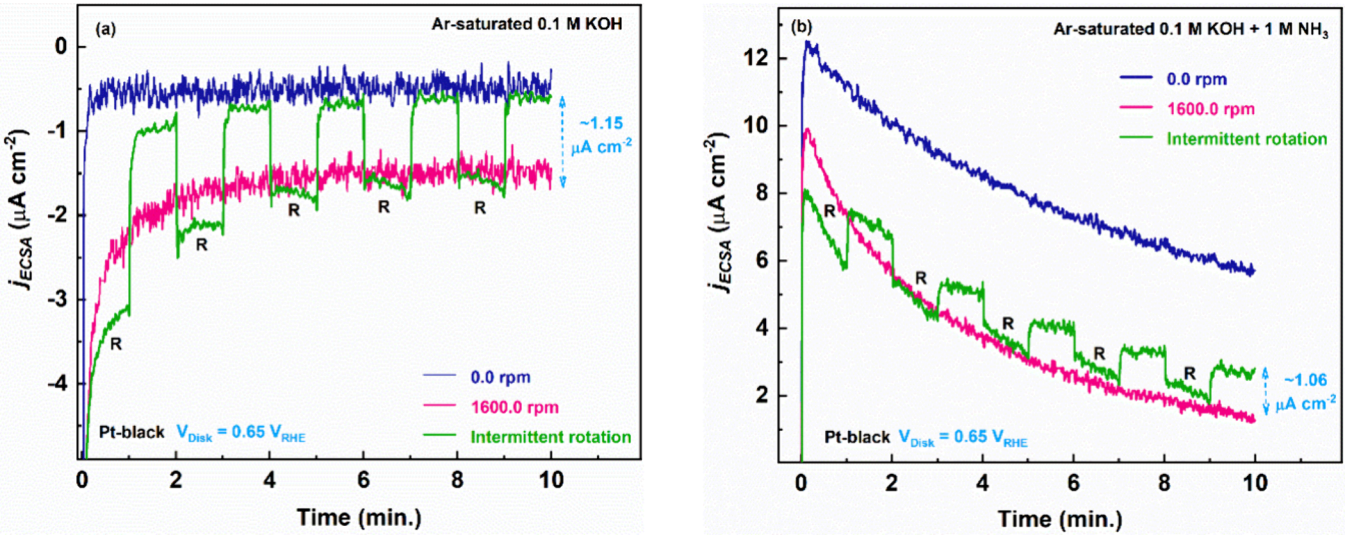


Figure 6. CAs on Pt-black at 0.65 V_{RHE} depicting the effect of intermittent rotation and convective mass transport in (a) 0.1 M KOH and (b) the same electrolyte containing 1.0 M NH_3. The label "R" denotes the period of rotation (1600.0 rpm) of the Pt-black electrode during intermittent rotation.

species, and consequently, a significant rise in the AOR current is recorded. Alongside NH_3 adsorption and dehydrogenation, the delayed reduction of Pt−$O_xH_yN_z$ is the major reason that suppresses A_4 in the 0.4 to 1.1 V range. Thus, AOR heavily depends on the presence of free Pt catalytic sites and the coverage of H_{ad}, $NH_{3,ad}$, and $O_xH_yN_z$ on Pt.

3.6. Chronoamperometry at Varying Mass Transport Conditions

Endo et al. performed an interesting set of chronoamperometric experiments by continuously varying the convective mass transport conditions to assess the effect of surface poisoning during AOR.[30] The system was switched from static to hydrodynamic mode by varying the disk electrode's rotation rate.

The results obtained from that experiment indicated a step response− i.e., the net oxidation current decreased instantly when the system became hydrodynamic and partially recovered as soon as the system became static. Since surface blocking by adsorbates causes an irreversible modification to the catalyst surface and the current recovery of a poisoned catalyst under static conditions is not expected, the extent of surface poisoning was concluded to be minimal. Instead, the fluctuating current with rotation was primarily attributed to the escape of the intermediates from the disk electrode.[30]

To test the above hypothesis, CAs of Pt-black were recorded under different mass-transport conditions in NH_3-free 0.1 M KOH electrolyte (Figure 6a). To begin with, the electrode was rotated at 1600.0 rpm for 60 s, followed by a rest (i.e., 0.0 rpm) for the next 60 s. The total duration of this experiment was 10 min, which was preceded by an induction period for 3 s. Although the currents obtained in Figure 6a are negative, and thus correspond to a cathodic process, a notable feature is consistently obtained as the disk electrode is rotated intermittently in 0.1 M KOH. The net current increases when the electrode is rotated and decreases immediately when the rotation is stopped.

On the basis of the observations, this feature is most likely a consequence of the reduction of oxygen species that are inherently dissolved in the electrolyte. Although the bulk electrolyte was purged with Ar for enough time before the experiment, there is a possibility of the presence of residual O_2 because of its incomplete removal. Thus, with an increase in the rotation rate, there is a renewed supply of the O_2 species to the disk electrode, leading to a visible increase in the reduction current. However, under static conditions, the extended diffusion layer and lack of O_2 near the electrode surface lead to a lower current.

Figure 6b corresponds to the same experiment in an NH_3-containing supporting electrolyte. A similar trend in the current was observed with intermittent rotation of the electrode.

In the presence of NH_3, the recorded data at both 0.0 and 1600.0 rpm demonstrate positive decaying currents, predominantly corresponding to NH_3 oxidation (Figure 6b). The decaying nature of the currents can be attributed to the formation of $O_xH_yN_z$ species that strongly binds to Pt and cause catalyst poisoning. Under conditions of intermittent rotation, a step response similar to that in Figure 6a is observed, having a comparable height of ~1−2 μA cm^{-2}. These features were previously attributed to the escape of AOR intermediates in the literature.[30] However, the presence of the step response in both NH_3-free and NH_3-containing electrolytes suggest that the step response is primarily driven

https://doi.org/10.1021/acs.jpcc.6c04500
J. Phys. Chem. C XXXX, XXX, XXX−XXX

Downloaded from pubs.acs.org/jpcccck/article-pdf/doi/10.1021/acs.jpcc.6c04500/6893061/acs.jpcc.6c04500.pdf by HIGHER COLLEGES OF TECHNOLOGY, Bradley Ladewig on 03 November 2026

by ORR with negligible contributions due to the escape of AOR intermediates.

To further verify the contributions from the dissolved O_2 content, chronoamperograms demonstrated in Figure 6 were repeated under various experimental conditions. The results presented in Figure S8 strongly indicate that the height of the step response is a function of the dissolved O_2 content; the step amplitude decreases systematically with reduced dissolved O_2 content in the electrolyte.

The complete elimination of dissolved O_2 content is practically not possible since minor O_2 re-entry can occur due to the open cell configuration and from the injection of NH_3 solution to the electrolyte (experimental evidence presented in Figure S9); in fact, the solubility of oxygen improves in the presence of NH_3.[46] Thus, the comparable step amplitudes (of the CAs under intermittent rotation), even after O_2 removal, can have contributions from incomplete deoxygenation and escape of N-derivatives of the form, $O_xH_yN_z$. Furthermore, at 0.65 V, Pt preferentially catalyzes ORR over AOR due to faster ORR kinetics. This observation is strengthened by the negative current corresponding to ORR in the chronoamperograms, even though the concentration of O_2 in O_2-saturated solutions (~1.2 mM, calculated via Henry's law and Sechenov's equation) is far lesser than that of NH_3, which is 1000 mM. Thus, even in the presence of NH_3, trace amounts of O_2 are significantly projected in the step responses.

3.7. RRDE Measurements of AOR on Pt-Black

RRDE voltammetry has been extensively used to evaluate electrocatalysis of ORR alongside the in situ detection and quantification of H_2O_2 intermediates.[47−49] Although RRDE-based studies are gaining prominence for other multistep multielectron reactions such as CO_2 reduction reaction (CO_2RR), the investigations for AOR remain sparse.[30,50,51] The present study extends the RRDE methodology to study the escape of intermediates under varying mass transport conditions during AOR.

To understand the characteristic underlying electrochemical processes associated with AOR, it is imperative to investigate the background voltammogram of the Pt-black-coated disk in an NH_3-free supporting electrolyte. Figure 7a presents the voltammograms of the Pt-black-coated disk electrode under static and rotating conditions of the disk electrode.

Figures 7b and 7c show i_{Ring} on Pt in NH_3-free supporting electrolyte under static and hydrodynamic conditions, respectively. The Pt ring was held at 0.45 V vs RHE during measurements. The currents were recorded after holding the disk electrode at 0.45 V in NH_3-free Ar-saturated electrolyte for 30 min to remove the dissolved O_2 content (details mentioned in the Experimental Section). As a result, the concentration of O_2 in the electrolyte becomes negligible, and the i_{Ring} at 0.0 rpm (corresponding to ORR) remains minor and steady due to mass transport limitations (Figure 7b).

On the other hand, under hydrodynamic conditions (1600.0 rpm) and enhanced mass transport, the unintentionally dissolved oxygen content of the bulk electrolyte readily reaches the ring and gets reduced. Thus, the obtained i_{Ring} has an enhanced contribution from ORR in contrast to the current obtained under static conditions (Figure 7b,c). Based on this, the i_{Ring} data in Figure 7c can be interpreted as follows. In the forward scan, the initial current appears to be steady over the range of ~0.05 to 0.75 V. At potentials higher than 0.75 V, an abrupt increase in the i_{Ring} is observed, coinciding with the

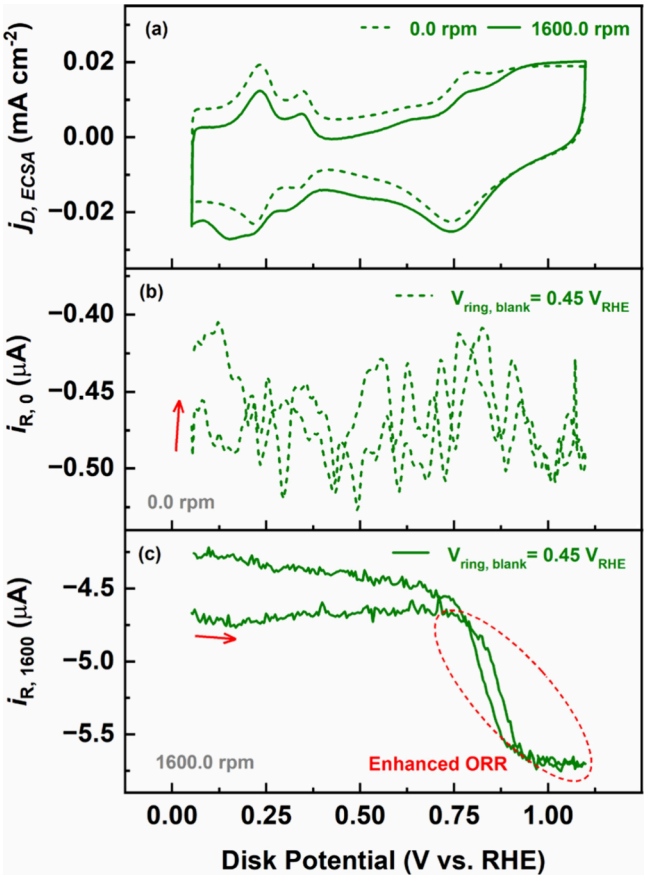


Figure 7. (a) CVs of Pt-black under static and hydrodynamic conditions of the disk electrode. (b) and (c) are the i_{Ring} recorded at 0.0 rpm (dashed line) and 1600.0 rpm (solid line). Arrows in the figure indicate the direction of the scan. All the curves are recorded in Ar-purged NH_3-free supporting electrolyte at 20 mV s^{-1}.

formation of surface oxides on the disk electrode. The formation of surface oxides at higher potentials inhibits the ability of Pt-black to catalyse ORR. This leads to an apparent increase in the oxygen content available to the ring electrode, and consequently, a prominent change in the cathodic i_{Ring} is recorded. Finally, a mass-transport limiting current is obtained as the disk potential crosses ~0.9 V.

In the reverse scan, as the surface oxides begin to reduce on the disk electrode, the catalytic sites of Pt-black become free, rendering a clean surface. This leads to renewed ORR on the disk surface, impeding the availability of O_2, and thus ORR at the ring at potentials of <1.15 V. At potentials of ~0.75 V, a crossover is observed in the i_{Ring}, which has been previously reported in the literature for ORR on Pt-black.[52,53] This hysteresis is attributed to the formation of a diffusion gradient and sudden availability of catalytic sites on the disk for ORR. As the disk potentials are further lowered, a steady i_{Ring} is obtained; however, it is slightly lower than the i_{Ring} in the forward scan due to an overall reduction in the available O_2 content.

Figure 8a and Figure 8a′ show the voltammograms of Pt-black in NH_3-free and NH_3-containing solutions, respectively, under hydrodynamic conditions. As discussed in Figure 2b, the j_{AOR}^{peak} is lower under hydrodynamic conditions (1600.0 rpm) as compared to that at static conditions. Studies in the literature attribute this to either increased poisoning of the active sites or escape of the intermediates (discussed in Figure 2).

https://doi.org/10.1021/acs.jpcc.6c04500
J. Phys. Chem. C XXXX, XXX, XXX−XXX

Downloaded from pubs.acs.org/jpcccck/article-pdf/doi/10.1021/acs.jpcc.6c04500/6893906l/acs.jpcc.6c04500.pdf by HIGHER COLLEGES OF TECHNOLOGY, Bradley Ladewig on 03 November 2026

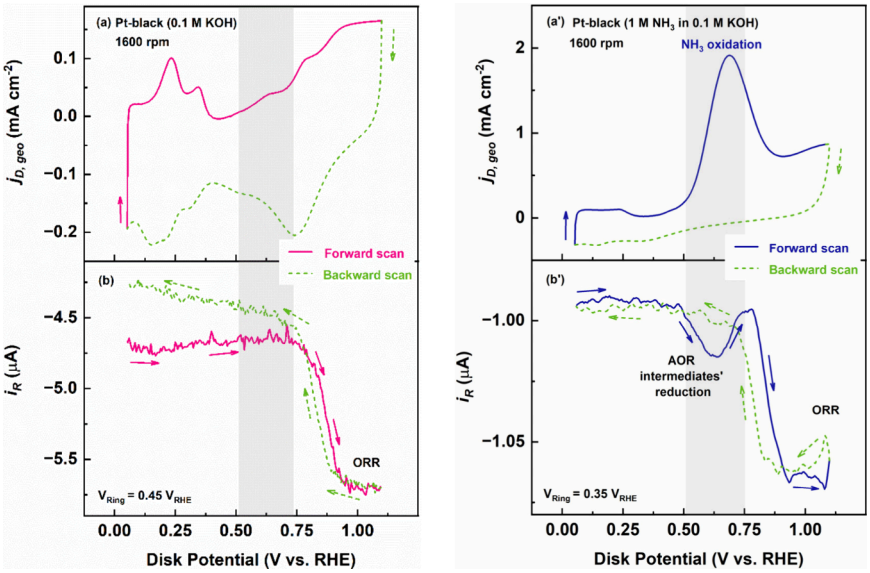


Figure 8. (a, a′) CVs of Pt-black in (a) NH_3-free and (a′) NH_3-containing solutions under hydrodynamic conditions. (b) and (b′) present the i_{Ring} recorded at 1600.0 rpm in NH_3-free and NH_3-containing solutions, respectively. Solid and dotted lines correspond to forward and backward scan, respectively, and arrows depict the direction of scan. All the data were recorded in electrochemically deoxygenated Ar-purged 0.1 M KOH electrolyte as a function of the disk potential at a scan rate of 20 mV s^{-1}.

To test the hypothesis of escaping intermediates with rotation, the i_{Ring} were recorded by holding the ring potential at 0.35 V in 1.0 M NH_3 containing electrolytes under static (Figure S10) and rotating (Figure 8b′) conditions of the electrode. The ring potentials correspond to the double layer-charging region on Pt-black in NH_3−free and NH_3 containing electrolyte. Since the onset for AOR in 1.0 M NH_3 is ∼0.36 V on Pt-black (from Figure 1b), the ring potentials are chosen such that the obtained currents are devoid of AOR contributions.

In Figures 8b 8, the initial i_{Ring} recorded up to ∼0.56 V (of the disk) corresponds to the reduction of the unintentionally dissolved O_2 content. However, the magnitude of the recorded current (up to ∼0.56 V) at static condition (0.0 rpm, Figure S10) is significantly higher than that at 1600.0 rpm. This difference is perhaps due to an increased supply of NH_3 and thereby a greater extent of NH_3 adsorption on the Pt ring when held at 0.35 V, eventually leading to a decrease in the number of free sites available to catalyze ORR.

As the disk potentials are further increased, a distinct reductive peak (i) appears on the ring in the potential range of 0.50 to 0.75 V under hydrodynamic conditions (1600 rpm, highlighted by the gray shaded area in Figure 8b′). Since no such feature is evident in NH_3-free electrolytes (Figure 8b), the results indicate the species involved are indeed N-based derivatives.

The adsorption of OH^- ions on Pt (>0.6 V) and formation of N-based derivatives ($O_xH_yN_z$) on Pt suggest that the reductive signal in the ring current corresponds to the reduction of N-based oxygenated species. Furthermore, several spectroscopic studies in the literature validate the Gerischer-Mauerer mechanism and hint at the formation of N_xH_y intermediates during AOR on the disk. On the basis of the existing literature reports and inferences from this study, the reductive signal detected on the ring current could correspond to either N_xH_y or $O_xH_yN_z$ species. The definitive identification of intermediates, however, is beyond the scope of this manuscript (due to experimental limitations) but can be investigated in future using *in situ* spectroscopic techniques.

Although the exact identity of the escaping intermediate is uncertain and requires rigorous *in situ* analysis, the detachment of N-based derivatives at higher rotation rates is evident from Figure 8b. This could perhaps also explain the declining j_{AOR}^{peak} under hydrodynamic conditions observed previously (Figure 2), arising from an increased contribution of i_{escape}^{-} in eq 3.

As previously discussed in Figure 7, the reductive feature (ii) obtained above 0.75 V corresponds to ORR. Likewise, a steady i_{ring} is obtained in the reverse scan due to the overall decrease in the available O_2 content, and the i_{ring} is slightly higher at 1600.0 rpm due to facile mass transport of O_2.

4. CONCLUSION

AOR is investigated on Pt-disk and Pt-black in 0.1 M KOH electrolyte using voltametric and chronoamperometric techniques in an RRDE configuration. The influence of ammonia concentration (1−1000 mM), rotation rate, upper- and lower-potential limits of the voltammograms, dissolved oxygen content, surface poisoning, and escape of intermediate species on AOR peak current are examined.

It is found that the AOR peak current is influenced mainly by the interplay among four factors: (i) convective mass transport, (ii) strong adsorption of certain species on the catalyst's active sites, (iii) the escape of weakly bound adsorbates from the electrode surface, and (iv) concomitant side reactions. The maximum AOR net current is obtained at ∼1.0 M NH_3 concentration under static conditions. NH_3 and its oxidation residues binds strongly to the Pt surface, and it alters the characteristic Pt voltametric features considerably, leading to a downshift in the potential of H adsorption/desorption, oxide reduction features, and enhanment of the capacitive contributions in the oxide formation region. This poisoning of the catalyst is one of the main factors inhibiting AOR activity and it is primarily driven by the strongly bound Pt−$O_xH_yN_z$ species formed at higher potential, as evidenced

https://doi.org/10.1021/acs.jpcc.6c04500
J. Phys. Chem. C XXXX, XXX, XXX−XXX

Downloaded from pubs.acs.org/jpcccck/article-pdf/doi/10.1021/acs.jpcc.6c04500/68939061/acs.jpcc.6c04500.pdf by HIGHER COLLEGES OF TECHNOLOGY, Bradley Ladewig on 03 November 2026

by the larger capacitive charges in the region of oxygenated species formation.

Characteristic features in the CA (under conditions of intermittent rotation) and ring current in the RRDE experiments indicate that the net current has contributions from both ammonia oxidation and oxygen reduction reactions. The intrinsic activity of ORR on Pt is superior to that of AOR such that it influences and alters the net AOR currents even at trace concentrations (where the NH_3:O_2 ratio is ~1000:1); the interference of ORR during AOR measurements has been often overlooked. The changes in the ring current features in the presence of NH_3 hint at the escape and consequent reduction of N-based derivatives (of the form, N_xH_y or $O_xH_yN_z$), however, it remains evasive about their exact identity.

The exact role of O_2 in AOR, the precise identities of the escaping N-derivatives and the poisoning species ($O_xH_yN_z$), and the mechanistic reason for the shift in H_{UPD} in the presence of NH_3 require further *in situ* spectroscopic investigations.

■ ASSOCIATED CONTENT

Supporting Information

The Supporting Information is available free of charge at https://pubs.acs.org/doi/10.1021/acs.jpcc.6c04500.

> Activation voltammograms of Pt-black in 0.5 M H_2SO_4 and 0.1 M KOH; procedure for preparing NH_3-containing supporting electrolytes; concentration dependence of AOR on Pt-disk and Pt-black; determination of Pt-black ECSA; effect of cycling of AOR on Pt-black; trend in AOR peak current on increasing NH_3 concentration from 0.5 mM to 1.0 M (effect of mass transport); electrode surface recovery in 0.5 M H_2SO_4; CA under different experimental conditions; solubility of O_2 in NH_3; RRDE data under static conditions (PDF)

■ AUTHOR INFORMATION

Corresponding Author

Manoj Neergat − *Department of Energy Science and Engineering, Indian Institute of Technology Bombay, Powai, Mumbai 400076, India;* orcid.org/0000-0003-1106-079X; Phone: +912225767893; Email: nmanoj@iitb.ac.in; Fax: +91 22 2576 4890

Authors

Amruta Iyer − *Department of Energy Science and Engineering, Indian Institute of Technology Bombay, Powai, Mumbai 400076, India;* orcid.org/0009-0005-6058-1710

Sagar Chauhan − *Department of Energy Science and Engineering, Indian Institute of Technology Bombay, Powai, Mumbai 400076, India;* orcid.org/0009-0004-2951-1231

Bradley P. Ladewig − *Paul Wurth Chair, Department of Engineering, Faculty of Science, Technology and Medicine, University of Luxembourg, Esch-sur-Alzette L-4365, Luxembourg;* Present Address: Technology and Science, Higher Colleges of Technology, United Arab Emirates; orcid.org/0000-0002-2135-1913

Complete contact information is available at: https://pubs.acs.org/10.1021/acs.jpcc.6c04500

Author Contributions

Amruta Iyer: conceptualization, methodology, data curation, formal analysis, writing—original draft, visualization. Sagar Chauhan: data curation, formal analysis, visualization. Bradley Ladewig: conceptualization. Manoj Neergat: conceptualization, formal analysis, writing—review and editing, supervision, funding acquisition.

Notes

The authors declare no competing financial interest.

■ ACKNOWLEDGMENTS

The National Centre for Photovoltaic Research and Education (NCPRE, RD/0122-MNRE000-001), funded by the Ministry of New and Renewable Energy, Science and Engineering Research Board (SERB, CRG/2022/003987), funded by the Department of Science and Technology (DST), Government of India, and Fonds National de la Recherche (RD/0123-LUXEM0A-001) are acknowledged for financial support of the project.

■ REFERENCES

(1) Adli, N. M.; Zhang, H.; Mukherjee, S.; Wu, G. Review-Ammonia Oxidation Electrocatalysis for Hydrogen Generation and Fuel Cells. *J. Electrochem. Soc.* **2018**, *165*, J3130−J3147.

(2) Vitse, F.; Cooper, M.; Botte, G. G. On the Use of Ammonia Electrolysis for Hydrogen Production. *J. Power Sources* **2005**, *142*, 18−26.

(3) López de Mishima, B. A.; Lescano, D.; Molina Holgado, T.; Mishima, H. T. Electrochemical Oxidation of Ammonia in Alkaline Solutions: Its Application to an Amperometric Sensor. *Electrochim. Acta* **1998**, *43*, 395−404.

(4) Marinčić, L.; Leitz, F. B. Electro-Oxidation of Ammonia in Waste Water. *J. Appl. Electrochem.* **1978**, *8*, 333−345.

(5) Qian, G.; Chen, J.; Jiang, W.; Yu, T.; Tan, K.; Yin, S. Strong Electronic Coupling of CoNi and N-Doped-Carbon for Efficient Urea-Assisted H_2 Production at a Large Current Density. *Carbon Energy* **2023**, *5*, No. e368.

(6) Hu, M.; Yu, T.; Tan, K.; Zhou, A.; Luo, L.; Yin, S. Ultralow Ru Loading RuO_2TiO_2 with Strong Oxide-Support Interaction for Efficient Chlorine Evolution and Ammonia-Nitrogen-Elimination. *Chem. Eng. J.* **2023**, *465*, No. 143001.

(7) Gerischer, H.; Mauerer, A. Untersuchungen zur anodischen Oxidation von Ammoniak an Platin-Elektroden. *J. Electroanal. Chem. Interfacial Electrochem.* **1970**, *25*, 421−433.

(8) Oswin, H. G.; Salomon, M. The Anodic Oxidation of Ammonia at Platinum Black Electrodes in Aqueous KOH Electrolyte. *Can. J. Chem.* **1963**, *41*, 1686−1694.

(9) Gootzen, J. F. E.; Wonders, A. H.; Visscher, W.; van Santen, R. A.; van Veen, J. A. R. A DEMS and Cyclic Voltammetry Study of NH_3 Oxidation on Platinized Platinum. *Electrochim. Acta* **1998**, *43*, 1851−1861.

(10) Herron, J. A.; Ferrin, P.; Mavrikakis, M. Electrocatalytic Oxidation of Ammonia on Transition-Metal Surfaces: A First-Principles Study. *J. Phys. Chem. C* **2015**, *119*, 14692−14701.

(11) Wasmus, S.; Vasini, E. J.; Krausa, M.; Mishima, H. T.; Vielstich, W. DEMS-Cyclic Voltammetry Investigation of the Electrochemistry of Nitrogen Compounds in 0.5 M Potassium Hydroxide. *Electrochim. Acta* **1994**, *39*, 23−31.

(12) de Vooys, A. C. A.; Koper, M. T. M.; van Santen, R. A.; van Veen, J. A. R. The Role of Adsorbates in the Electrochemical Oxidation of Ammonia on Noble and Transition Metal Electrodes. *J. Electroanal. Chem.* **2001**, *506*, 127−137.

(13) Finkelstein, D. A.; Bertin, E.; Garbarino, S.; Guay, D. Mechanistic Similarity in Catalytic N_2 Production from NH_3 and NO_2^- at Pt (100) Thin Films: Toward a Universal Catalytic Pathway

Downloaded from pubs.acs.org/jpccck/article-pdf/doi/10.1021/acs.jpcc.6c04500/6893906l/acs.jpcc.6c04500.pdf by HIGHER COLLEGES OF TECHNOLOGY, Bradley Ladewig on 03 November 2026

for Simple N-Containing Species, and Its Application to In Situ Removal of NH_3 Poisons. *J. Phys. Chem. C* **2015**, *119*, 9860−9872.
(14) Katsounaros, I.; Chen, T.; Gewirth, A. A.; Markovic, N. M.; Koper, M. T. M. Evidence for Decoupled Electron and Proton Transfer in the Electrochemical Oxidation of Ammonia on Pt (100). *J. Phys. Chem. Lett.* **2016**, *7*, 387−392.
(15) Rosca, V.; Koper, M. T. M. Electrocatalytic Oxidation of Ammonia on Pt (111) and Pt (100) Surfaces. *Phys. Chem. Chem. Phys.* **2006**, *8*, 2513−2524.
(16) Vidal-Iglesias, F. J.; Solla-Gullón, J.; Montiel, V.; Feliu, J. M.; Aldaz, A. Ammonia Selective Oxidation on Pt (100) Sites in an Alkaline Medium. *J. Phys. Chem. B* **2005**, *109*, 12914−12919.
(17) Shi, W.; Liu, S.; Zhang, L.; Zhou, F.; Shen, W.; Huang, P.; Ge, M.; Yuan, X.; Qian, T. Site-Differentiated Self-Assembled PtMn Nanocluster Shells Enable Dual-Site Ammonia Oxidation in Direct Ammonia Fuel Cells. *Nano Lett.* **2026**, *26*, 9066−9075.
(18) Yu, T.; Tan, K.; Wu, J.; Zou, Y.; Yin, S. Bifunctional Interstitial Phosphorous Doping Strategy Boosts Platinum-Zinc Alloy for Efficient Ammonia Oxidation Reaction and Hydrogen Evolution Reaction. *Nano Res.* **2024**, *17*, 1182−1189.
(19) Novell-Leruth, G.; Ricart, J. M.; Pérez-Ramírez, J. Pt (100)-Catalyzed Ammonia Oxidation Studied by DFT: Mechanism and Microkinetics. *J. Phys. Chem. C* **2008**, *112*, 13554−13562.
(20) Katsounaros, I.; Figueiredo, M. C.; Calle-Vallejo, F.; Li, H.; Gewirth, A. A.; Markovic, N. M.; Koper, M. T. M. On the Mechanism of the Electrochemical Conversion of Ammonia to Dinitrogen on Pt (100) in Alkaline Environment. *J. Catal.* **2018**, *359*, 82−91.
(21) Kim, H.; Kim, D.; Bang, J.; Hong, S.; Park, H.; Ahn, S. H. Atomic-Scale Ir Decoration on Pt (100) via Self-Terminated Electrodeposition for Electrochemical Ammonia Oxidation. *Chem. Eng. J.* **2026**, *545*, No. 179698.
(22) Endo, K.; Nakamura, K.; Katayama, Y.; Miura, T. Pt-Me (Me = Ir, Ru, Ni) Binary Alloys as an Ammonia Oxidation Anode. *Electrochim. Acta* **2004**, *49*, 2503−2509.
(23) Najafian, A.; Cundari, T. R. Computational Mechanistic Study of Electro-Oxidation of Ammonia to N_2 by Homogenous Ruthenium and Iron Complexes. *J. Phys. Chem. A* **2019**, *123*, 7973−7982.
(24) Zott, M. D.; Garrido-Barros, P.; Peters, J. C. Electrocatalytic Ammonia Oxidation Mediated by a Polypyridyl Iron Catalyst. *ACS Catal.* **2019**, *9*, 10101−10108.
(25) Little, D. J.; Edwards, D. O.; Smith, M. R.; Hamann, T. W. As Precious as Platinum: Iron Nitride for Electrocatalytic Oxidation of Liquid Ammonia. *ACS Appl. Mater. Interfaces* **2017**, *9*, 16228.
(26) Liu, H. Y.; Lant, H. M. C.; Troiano, J. L.; Hu, G.; Mercado, B. Q.; Crabtree, R. H.; Brudvig, G. W. Electrocatalytic, Homogeneous Ammonia Oxidation in Water to Nitrate and Nitrite with a Copper Complex. *J. Am. Chem. Soc.* **2022**, *144*, 8449−8453.
(27) Offen-Polak, I.; Ayali Aviram, H.; Hijaze, A.; Slot, T. K.; Eisenberg, D. Ammonia Electro-Oxidation on Nickel Hydroxide: Phases, pH and Poisoning. *Phys. Chem. Chem. Phys.* **2025**, *27*, 10949−10961.
(28) Kapałka, A.; Cally, A.; Neodo, S.; Comninellis, C.; Wächter, M.; Udert, K. M. Electrochemical Behavior of Ammonia at Ni/$Ni(OH)_2$ Electrode. *Electrochem. Commun.* **2010**, *12*, 18−21.
(29) Shih, Y. J.; Huang, Y. H.; Huang, C. P. Electrocatalytic Ammonia Oxidation over a Nickel Foam Electrode: Role of $Ni(OH)_2$(s)-NiOOH(s) Nanocatalysts. *Electrochim. Acta* **2018**, *263*, 261−271.
(30) Endo, K.; Katayama, Y.; Miura, T. A Rotating Disk Electrode Study on the Ammonia Oxidation. *Electrochim. Acta* **2005**, *50*, 2181−2185.
(31) Neergat, M.; Shukla, A. K.; Gandhi, K. S. Platinum-Based Alloys as Oxygen-Reduction Catalysts for Solid-Polymer-Electrolyte Direct Methanol Fuel Cells. *J. Appl. Electrochem.* **2001**, *31*, 373−378.
(32) Bard, A. J.; Faulkner, L. R.. *Electrochemical Methods: Fundamentals and Applications*, 2nd ed.; John Wiley & Sons: New York, 2001.
(33) Trasatti, S.; Petrii, O. A. Real Surface Area Measurements in Electrochemistry. *Pure Appl. Chem.* **1991**, *63*, 711−734.
(34) Bunce, N. J.; Bejan, D. Mechanism of Electrochemical Oxidation of Ammonia. *Electrochim. Acta* **2011**, *56*, 8085−8093.
(35) Devivaraprasad, R.; Kar, T.; Chakraborty, A.; Singh, R. K.; Neergat, M. Reconstruction and Dissolution of Shape-Controlled Pt Nanoparticles in Acidic Electrolytes. *Phys. Chem. Chem. Phys.* **2016**, *18*, 11220−11232.
(36) Feliu, J. M.; Herrero, E. Pt Single Crystal Surfaces in Electrochemistry and Electrocatalysis. *EES Catal.* **2024**, *2*, 399−418.
(37) Palaniappan, R.; Ingram, D. C.; Botte, G. G. Hydrogen Evolution Reaction Kinetics on Electrodeposited Pt-M (M = Ir, Ru, Rh, and Ni) Cathodes for Ammonia Electrolysis. *J. Electrochem. Soc.* **2014**, *161*, E12−E22.
(38) Paliwal, A.; Assaf, L.; Long, H.; Haasch, R. T.; Gupta, J. K.; Reynolds, M. A.; Son, Y. J.; Zhang, K.; Kenis, P. J. A.; Gewirth, A. A. Mechanistic Insights into the Enhanced Ammonia Oxidation Activity of PtRh Electrodeposits. *ACS Appl. Mater. Interfaces* **2025**, *17*, 3383−3392.
(39) Jerkiewicz, G.; Deblois, M.; Radovic-Hrapovic, Z.; Tessier, J. P.; Perreault, F.; Lessard, J. Underpotential Deposition of Hydrogen on Benzene-Modified Pt (111) in Aqueous H_2SO_4. *Langmuir* **2005**, *21*, 3511−3520.
(40) Vidal-Iglesias, F. J.; Solla-Gullón, J.; Feliu, J. M.; Baltruschat, H.; Aldaz, A. DEMS Study of Ammonia Oxidation on Platinum Basal Planes. *J. Electroanal. Chem.* **2006**, *588*, 331−338.
(41) Wang, H.; Dekel, D. R.; Abruña, H. D. Unraveling the Mechanism of Ammonia Electrooxidation by Coupled Differential Electrochemical Mass Spectrometry and Surface-Enhanced Infrared Absorption Spectroscopic Studies. *J. Am. Chem. Soc.* **2024**, *146*, 15926−15940.
(42) Gupta, G.; Choudhury, D.; Maurya, R.; Sharma, S.; Neergat, M. Investigation of Hydrogen Oxidation/Evolution Reactions Based on Charge-Transfer Coefficients Derived from Butler-Volmer and Eyring Analyses. *J. Phys. Chem. C* **2023**, *127*, 23566−23576.
(43) Devivaraprasad, R.; Kar, T.; Leuaa, P.; Neergat, M. Recovery of Active Surface Sites of Shape-Controlled Platinum Nanoparticles Contaminated with Halide Ions and Its Effect on Surface-Structure. *J. Electrochem. Soc.* **2017**, *164*, H551−H560.
(44) Marković, N. M.; Gasteiger, H. A.; Ross, P. N. Oxygen Reduction on Platinum Low-Index Single-Crystal Surfaces in Alkaline Solution: Rotating Ring-Disk Pt (hkl) Sudies. *J. Phys. Chem.* **1996**, *100*, 6715−6721.
(45) García-Araez, N.; Climent, V.; Rodríguez, P.; Feliu, J. M. Thermodynamic Evidence for K^+-SO_4^{2-} Ion Pair Formation on Pt (111). New Insight into Cation Specific Adsorption. *Phys. Chem. Chem. Phys.* **2010**, *12*, 12146−12152.
(46) Tromans, D. Oxygen Solubility Modelling in Ammoniacal Leaching Solutions: Leaching of Sulphide Concentrates. *Miner. Eng.* **2000**, *13*, 497.
(47) Das, R.; Choudhury, D.; Maurya, R.; Sharma, S.; Neergat, M. Influence of Nitrogen Doping into Carbon on the Activation Barrier of ORR in Alkaline Medium: An Investigation Based on Eyring Analysis. *Langmuir* **2023**, *39*, 4351−4361.
(48) Singh, R. K.; Rahul, R.; Neergat, M. Stability Issues in Pd-Based Catalysts: The Role of Surface Pt in Improving the Stability and Oxygen Reduction Reaction (ORR) Activity. *Phys. Chem. Chem. Phys.* **2013**, *15*, 13044−13051.
(49) Paulus, U. A.; Schmidt, T. J.; Gasteiger, H. A.; Behm, R. J. Oxygen Reduction on a High-Surface Area Pt/Vulcan Carbon Catalyst: A Thin-Film Rotating Ring-Disk Electrode Study. *J. Electroanal. Chem.* **2001**, *495*, 134−145.
(50) Goyal, A.; Marcandalli, G.; Mints, V. A.; Koper, M. T. M. Competition between CO_2 Reduction and Hydrogen Evolution on a Gold Electrode under Well-Defined Mass Transport Conditions. *J. Am. Chem. Soc.* **2020**, *142*, 4154−4161.
(51) Zhang, F.; Co, A. C. Direct Evidence of Local pH Change and the Role of Alkali Cation during CO_2 Electroreduction in Aqueous Media. *Angew. Chem., Int. Ed.* **2020**, *59*, 1674−1681.

Downloaded from pubs.acs.org/jpccck/article-pdf/doi/10.1021/acs.jpcc.6c04500/6893906l/acs.jpcc.6c04500.pdf by HIGHER COLLEGES OF TECHNOLOGY, Bradley Ladewig on 03 November 2026

https://doi.org/10.1021/acs.jpcc.6c04500
J. Phys. Chem. C XXXX, XXX, XXX−XXX

(52) Van Brussel, M.; Kokkinidis, G.; Hubin, A.; Buess-Herman, C. Oxygen Reduction at Platinum Modified Gold Electrodes. *Electrochim. Acta* **2003**, *48*, 3909−3919.
(53) Conway, B. E. Electrochemical Oxide Film Formation at Noble Metals as a Surface-Chemical Process. *Prog. Surf. Sci.* **1995**, *49*, 331−452.

Downloaded from pubs.acs.org/jpccck/article-pdf/doi/10.1021/acs.jpcc.6c04500/6893906l/acs.jpcc.6c04500.pdf by HIGHER COLLEGES OF TECHNOLOGY, Bradley Ladewig on 03 November 2026

https://doi.org/10.1021/acs.jpcc.6c04500
J. Phys. Chem. C XXXX, XXX, XXX−XXX